


Article

# Development of Predictive Models for Tempering Behavior in Low-Carbon Bainitic Steel Using Integrated Tempering Parameters

Guojin Sun <sup>1,\*</sup> and Qi Wang <sup>2</sup> <sup>1</sup> School of Engineering, Qinghai Institute of Technology, Xining 810016, China<sup>2</sup> Electrical Engineering Division, Department of Engineering, University of Cambridge, Cambridge CB3 0FA, UK; qw273@cam.ac.uk

\* Correspondence: guojinsun@qh.it.edu.cn

**Abstract:** Low-carbon bainitic steels are known for their excellent combination of strength and toughness, making them suitable for various industrial applications. Understanding the tempering behavior of these steels is crucial for optimizing their mechanical properties through heat treatment. This study presents predictive models for tempering behavior based on empirical data, which is fundamental for understanding the thermal stability and transformation kinetics of the steel. Through integrated tempering parameters, we established predictive models that integrate tempering temperature and time, yielding a robust framework for predicting hardness. The equivalent tempering kinetic curves and nomographs plotted in this study allow for the direct determination of hardness under various tempering conditions, facilitating the optimization of tempering parameters. The nomogram approach provides a practical method for adjusting tempering parameters to achieve desired mechanical properties efficiently. The accuracy of the predictive models was validated through statistical tests, demonstrating a high correlation between predicted and experimental values.

**Keywords:** tempering process; predictive model; mechanical properties; low-carbon bainitic steels; tempering parameters optimization



**Citation:** Sun, G.; Wang, Q. Development of Predictive Models for Tempering Behavior in Low-Carbon Bainitic Steel Using Integrated Tempering Parameters. *Metals* **2024**, *14*, 881. <https://doi.org/10.3390/met14080881>

Academic Editors: Koh-ichi Sugimoto, Tomohiko Hojo and Junya Kobayashi

Received: 15 July 2024

Revised: 28 July 2024

Accepted: 29 July 2024

Published: 30 July 2024



**Copyright:** © 2024 by the authors. Licensee MDPI, Basel, Switzerland. This article is an open access article distributed under the terms and conditions of the Creative Commons Attribution (CC BY) license (<https://creativecommons.org/licenses/by/4.0/>).

## 1. Introduction

The application of advanced smelting technology significantly reduces impurities such as sulfur (S) and phosphorus (P) in steel, resulting in higher purity and cleanliness of the liquid steel [1–4]. This technological advancement has paved the way for the development of low-carbon high strength bainitic steel, which exemplifies the benefits of pure smelting techniques [5,6]. The enhanced properties of this steel are achieved through a combination of fine-grain strengthening, sub-structural strengthening, micro-alloying, and precipitation strengthening. These methods contribute to the steel's excellent mechanical properties, such as superior strength and toughness, making it ideal for demanding applications [7,8].

The significance of bainitic steel lies in its ability to maintain high strength and toughness under various conditions. This is particularly beneficial for high-performance structures and components, where material failure could have catastrophic consequences. For instance, in the construction of bridges, the robustness and durability of bainitic steel ensure long-term reliability and safety. Similarly, in the fabrication of oil platforms, this steel provides the necessary resilience to withstand harsh marine environments and extreme weather conditions. The shipbuilding industry also relies on bainitic steel to deliver ships that are not only strong but also capable of withstanding the rigors of sea voyages, including corrosive sea water and mechanical stress.

Moreover, the ongoing research and development in smelting and alloying techniques continue to enhance the properties of bainitic steel, pushing the boundaries of its applications. The integration of cutting-edge technologies in the production process not only improves the steel's performance but also makes it more cost-effective and environmentally friendly. As industries strive for materials that offer a balance between performance

and sustainability, low-carbon high-strength bainitic steel stands out as a prime example of modern metallurgical innovation. This progress underscores the critical role of advanced smelting technologies in meeting the evolving demands of high-performance engineering applications.

Research on the effect of carbon content on bainitic steels began in the 1960s [9]. To improve the hardenability of low-carbon bainitic steels, researchers added manganese (Mn) along with suitable amounts of boron (B) and titanium (Ti) to the steel, achieving tensile strengths up to 1000 MPa [10]. Further investigations delved into the specifics of manganese content and its effects on the properties of bainitic steels. These studies culminated in the development of a Mn-B alloy system tailored for air-cooled bainitic steel, highlighting the critical role of Mn in enhancing the steel's hardenability and mechanical properties [11–13]. This Mn-B alloy system has proven particularly effective, enabling the production of steels with exceptional strength and toughness suitable for demanding industrial applications. Significant contributions to this field have been made by Caballero and colleagues, who examined the impact of varying carbon content on bainitic steels. Their research demonstrated that increasing the carbon content to 0.4% can elevate the tensile strength of bainitic steel to over 1375 MPa. However, this impressive increase in strength came at the cost of reduced toughness, necessitating further treatments to balance these properties. Tempering treatments became essential to mitigate the brittleness induced by higher carbon content, ensuring the steel maintained adequate toughness for practical applications [14–18].

These foundational studies underscore the complex interplay between alloying elements and carbon content in determining the mechanical properties of bainitic steels. They also highlight the ongoing need for precise control over the composition and heat treatment processes to optimize these materials for high-performance applications. Research efforts from the 1960s onwards have paved the way for the development of advanced bainitic steels, tailored to meet the stringent demands of modern engineering and industrial applications. To ensure the optimal mechanical properties of steel, heat treatments such as quenching, normalizing, and tempering are often required [19,20]. Among these, tempering stands out as the final and most crucial heat treatment process. The success of tempering largely depends on the precise selection of temperature and time parameters; incorrect selections can adversely affect the mechanical properties of steel, including inducing temper brittleness, altering hardness, and reducing impact toughness. Therefore, the establishment of reliable tempering prediction models is vital for optimizing these parameters and predicting the resulting mechanical properties.

Holloman and Jaffe made significant contributions to this field by proposing a numerical relationship that predicts the mechanical properties of steels post-tempering. This relationship has been expressed in various forms by different authors [21–24]. Their model ingeniously integrates tempering temperature and time into a single  $P$  tempering parameter, effectively capturing the combined influence of these variables on the tempering process [25–27]. This parameter is calculated using the Hollomon-Jaffe equation, which primarily depends on the carbon content in the steel and can be determined through empirical formulas. This  $P$  tempering parameter has proven to be a reliable predictor of the mechanical outcomes of tempering. Due to the fact that the  $P$  tempering parameter only considers the carbon content and uses a look-up table for its calculation, without accounting for the effects of other alloying elements, other researchers have been prompted to seek alternative tempering prediction parameters. In parallel, Inoue developed a similar parameter, designated as the  $\lambda$  tempering parameter, to quantify the degree of tempering progress during heating and soaking processes [28–31]. The  $\lambda$  tempering parameter, derived from experimental data and statistical analysis, provides a more accurate representation of the material's tempering process. The  $\lambda$  tempering parameter provides a quantitative measure of the degree of tempering by incorporating the activation energy into its calculation. This parameter allows for a more comprehensive understanding of the tempering process by accounting for the energy required for atomic movements and transformations during

tempering. Once the  $\lambda$  tempering parameter is determined for specific temperature and time conditions, it can be used to predict the mechanical properties of steels during the tempering process. This parameter-based approach allows for a more nuanced and accurate prediction of how different tempering conditions will affect the steel.

The objective of this study is to investigate the tempering behavior of low-carbon bainitic steel, with a particular focus on the key parameters of tempering temperature and time. By developing mechanical prediction models based on the  $P$  and  $\lambda$  tempering parameters, this research aims to optimize the tempering parameters and accurately predict the mechanical properties of the steel during the tempering process. Through statistical methods, the tempering activation energy of the steel is calculated, and kinetic curves for hardness equivalents are plotted alongside a nomograph for tempering process parameters.

## 2. Experimental Procedure

The material investigated in this study is a low-carbon bainitic steel, with its primary chemical composition detailed in Table 1. Following controlled rolling and cooling, specimens measuring 15 mm × 15 mm × 20 mm were prepared. The rolling process commenced at an initial temperature of 1050 °C and concluded at 800 °C. Subsequently, the samples underwent tempering at temperatures ranging from 200 °C to 700 °C for durations of 0.5 h, 1.0 h, 1.5 h, and 2.0 h.

**Table 1.** Main chemical composition of steel (mass fraction, %).

Element	C	Si	Mn	P	S	Ni	Nb	Cr	Mo	Fe
Content	0.04	0.25	1.6	<0.006	<0.006	<1.0	0.015–0.07	<0.7	<0.5	Rest (up to 100%)

Post-tempering, the samples were subjected to a grinding and polishing process, followed by etching with a 4% nitric alcohol solution to reveal the microstructure. The microstructural examination was conducted using scanning electron microscopy (SEM), providing detailed images of the steel's microstructure. To obtain high-resolution images, the scanning electron microscope (SEM) was operated with an accelerating voltage of 18 kV and a working distance of 12 mm. This setup ensured optimal imaging conditions for detailed microstructural analysis. The hardness of the samples was measured using an HVS-1000 microhardness tester (Vickers, London, UK), ensuring precise and accurate measurements. The Vickers hardness tests were performed using a standard load of 1 kgf and a dwell time of 10 s. This method ensures consistent and accurate measurements of hardness, which are critical for analyzing the effects of tempering parameters on the mechanical properties of low-carbon bainitic steels.

Based on the obtained hardness values, a tempering prediction model and tempering kinetic curves for the steel were developed. These models are crucial for understanding the tempering behavior and optimizing the tempering parameters for the steel. The comprehensive data collected from these procedures provide a robust foundation for further analysis and validation of the tempering models.

## 3. Results and Discussion

### 3.1. Effect of Tempering Parameters on Hardness

Hardness measurements were taken at a minimum of ten distinct positions on each specimen after tempering at various temperatures and durations. For each tempering process, at least three microhardness measurements were taken for each sample. If the hardness deviation exceeded 5 HV, an additional three measurements were performed to ensure accuracy. This rigorous measurement protocol ensures the reliability and consistency of the hardness data, which is critical for the subsequent analysis and validation of the tempering models. The additional measurements help to account for any potential variations in the material's microstructure and provide a more accurate representation of the material's mechanical properties after tempering. The final hardness value for each

sample was determined by averaging the measurements and excluding any outliers to ensure accuracy. The influence of tempering temperature and time on the hardness of the steel is illustrated in Figure 1.

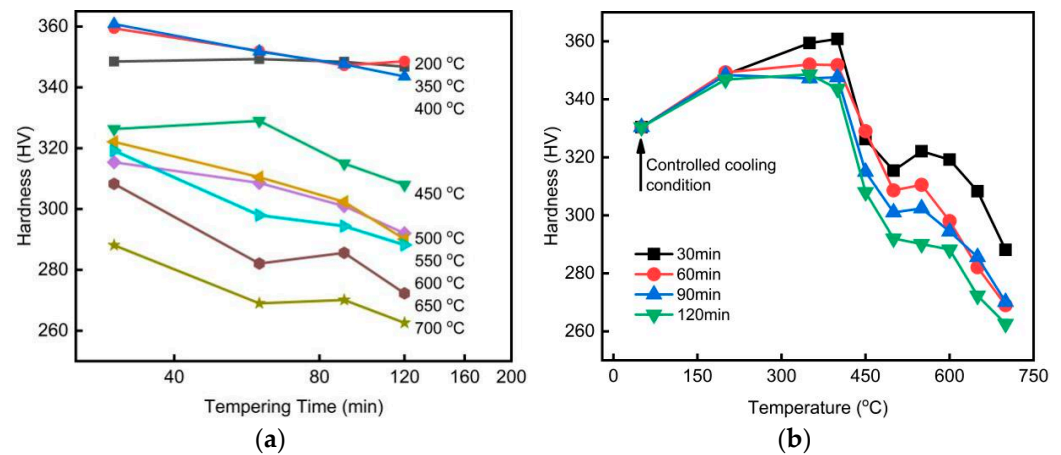


**Figure 1.** Effect of tempering parameters on the hardness of steel: (a) effect of tempering time; (b) effect of tempering temperature.

The results, depicted in Figure 1, indicate that the hardness of low-carbon bainitic steel generally decreases with increasing tempering time. This decrease follows a linear relationship with the logarithm of tempering time. However, the effect of tempering temperature on hardness is more complex. At lower tempering temperatures, hardness initially increases, reaching a peak at around 400 °C. Beyond this temperature, hardness begins to decrease. A slight secondary hardening is observed at approximately 550 °C, after which the hardness decreases sharply with further increases in temperature. These variations in hardness are closely related to the microstructural changes occurring during tempering. At lower tempering temperatures, residual austenite decomposes, leading to an initial increase in hardness. As tempering temperature increases, martensitic decomposition occurs alongside residual austenite decomposition, causing hardness to increase further. The secondary hardening observed at 550 °C is likely due to the precipitation of NbC particles, as supported by findings from other researchers [32,33]. At temperatures above 550 °C, the rapid decrease in hardness is due to the complete decomposition of martensite and the coarsening of carbides, along with the formation of massive ferrite, which contributes to the reduction in hardness. These findings highlight the importance of carefully selecting tempering parameters to achieve desired mechanical properties in low-carbon bainitic steels.

The purpose of tempering is to improve the toughness and plasticity of quenched steel and to eliminate residual stresses from the quenching process. Therefore, overall, as the tempering temperature increases and the tempering time extends, the hardness of the material generally shows a decreasing trend. The microstructural transformations mainly include the decomposition of martensite, the precipitation of carbides, and the growth of these carbides. We observed the effect of tempering for 30 min on the microstructure of the steel, with the results illustrated in Figure 2. This analysis provides a simple understanding of how tempering time influences the microstructure and, consequently, the mechanical properties of the steel.

As depicted in Figure 2a,b, the microstructures after low-temperature tempering show no significant differences compared to those under initial water-cooling conditions. This indicates that the low-temperature tempering process does not induce substantial microstructural changes. However, during low-temperature tempering, the transformation and decomposition of residual austenite lead to an initial increase in hardness [34,35]. This phenomenon can be attributed to the stabilization of retained austenite, which transforms into martensite during cooling. As the tempering temperature rises, the hardness of the steel



continues to increase due to the further decomposition of residual austenite. Concurrently, a decrease in hardness is observed due to the decomposition of martensite. This dual effect creates a complex interplay between hardening and softening mechanisms. However, as the temperature continues to rise to 550 °C (Figure 2c), a slight secondary hardening phenomenon is observed. This phenomenon, as referenced by other scholars' research findings, is likely caused by the precipitation of carbides such as NbC. The presence of NbC particles has been identified as a factor contributing to this secondary hardening effect, enhancing the steel's mechanical properties at this specific temperature [32,33]. This understanding aligns with the established theories on carbide precipitation and its impact on the hardness of tempered steels. The comprehensive data and the alignment with existing studies further validate our observations and provide a robust foundation for optimizing tempering processes. When the tempering temperature exceeds 550 °C, a sharp decrease in hardness is observed. This decline is due to the complete decomposition of martensite, which reduces the steel's overall hardness. Additionally, the coarsening of carbides at high temperatures further contributes to the reduction in hardness. The emergence of massive ferrite, as indicated by the arrow in Figure 2d, plays a significant role in this process. Ferrite is a relatively soft phase, and its formation leads to a pronounced decrease in hardness.

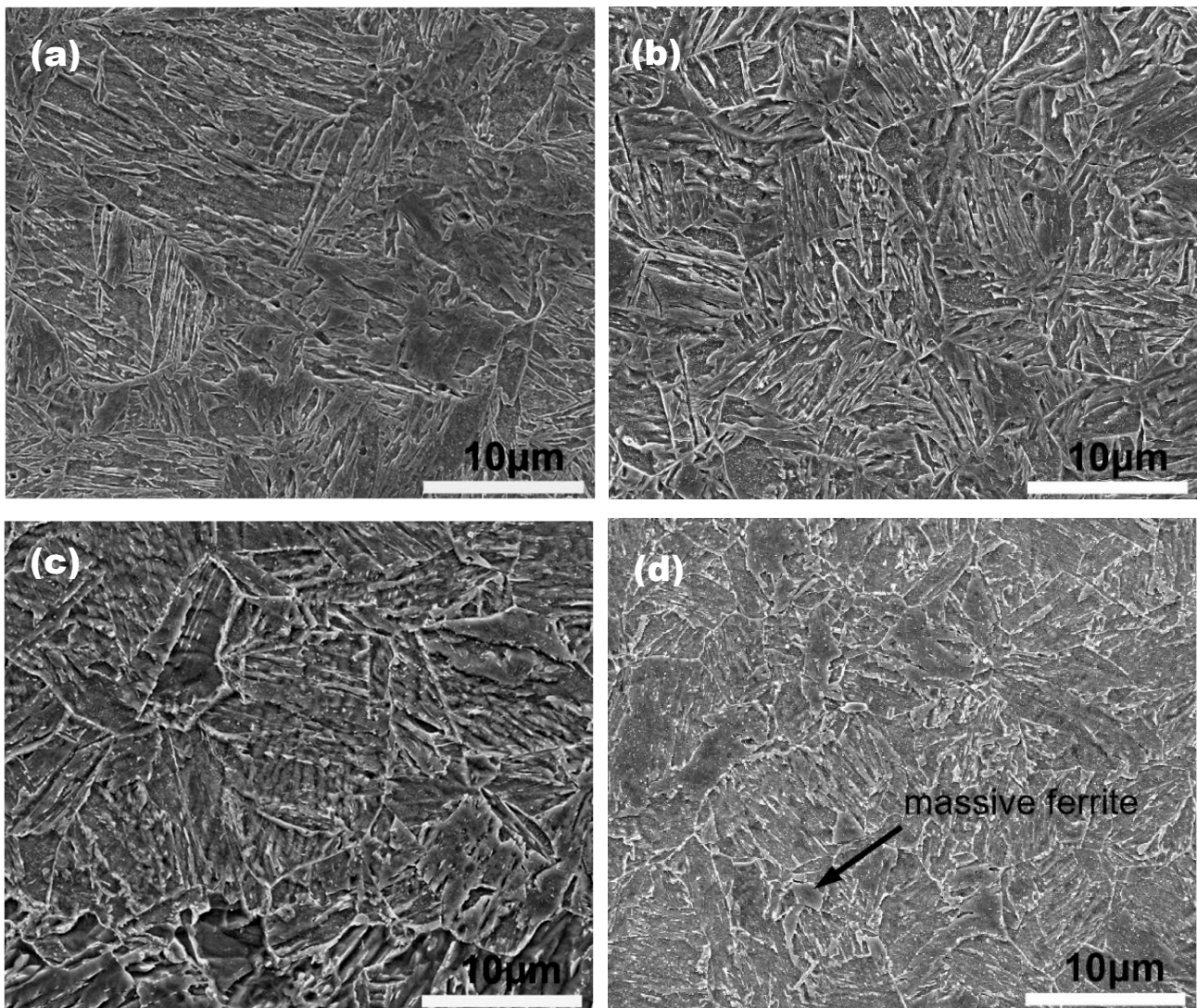


**Figure 2.** Effect of tempering temperatures on the microstructure of steel: (a) initial water cooling stage; (b) tempered at 200 °C; (c) tempered at 550 °C; (d) tempered at 600 °C.

### 3.2. Establishment of Tempering Model Based on $\lambda$ and $P$ Tempering Parameters

Tempering steel is a solid-state reaction process that involves the diffusive movement of atoms activated by heat. Inoue proposed a  $\lambda$  tempering parameter to describe the degree of tempering progress [25]. This parameter indicates the extent to which the tempering process has been influenced by time and temperature. It is derived as follows:

$$C = \gamma \cdot t = At \exp\left(\frac{Q}{RT}\right) \quad (1)$$

$$\lg C = \lg t - \left(\frac{Q}{2.3R}\right)\left(\frac{1}{T}\right) + \lg(A) \quad (2)$$

where:

$A$  is the pre-exponential factor,

$t$  is the tempering time (h),

$Q$  is the activation energy during the tempering process,

$R$  is the ideal gas constant (1.99 cal/mol),

$T$  is the tempering temperature (K).

To represent  $\lg C$  and utilize these assumptions, we derive a typical expression:

$$\lambda = \lg t - \left(\frac{Q}{2.3R}\right)\left(\frac{1}{T}\right) + 50 \quad (3)$$

It is evident that the parameter  $\lambda$  has a direct impact on the properties after tempering. The mechanical properties, such as hardness, are dependent on the  $\lambda$  tempering parameter, where:

$$M = f(\lambda) = f\left[\lg t - \left(\frac{Q}{2.3R}\right)\left(\frac{1}{T}\right) + 50\right] \quad (4)$$

To simplify calculations, it is assumed that:

$$M = a \lg t + b\left(\frac{1}{T}\right) + c \quad (5)$$

$$M = a\left[\lg t + \left(\frac{b}{a}\right)\left(\frac{1}{T}\right) + 50\right] - 50a + c \quad (6)$$

Compare Equation (6) and Equation (3):

$$Q = 2.3R\left(\frac{b}{a}\right) \quad (7)$$

The values for  $a$ ,  $b$ , and  $c$  are determined using the least squares method by substituting various temperatures, times, and hardness values into Equation (5). The activation energy and tempering model for the steel in this study have been calculated as follows:

$$\begin{aligned} M &= 11.96 - 24.54 \lg t + 2.22 \times 10^5 \left(\frac{1}{T}\right) \\ Q &= 2.3R\left(\frac{b}{a}\right) = 41.63 \text{ (kcal/mol)} \end{aligned} \quad (8)$$

Holloman and Jaffe proposed a prediction model for steel after the tempering process [21]. The equation commonly referred to as the Holloman-Jaffe equation is as follows:

$$P = T(K + \lg t) \quad (9)$$

where:

$P$  is the tempering parameter,

$t$  is the tempering time (h),

$T$  is the tempering temperature (K),

$K$  is a material-dependent constant.

For low-carbon bainitic steel, the constant ( $K$ ) is related to the carbon content, determined as follows:

$$K = 21.3 - 5.8 \times (C\%wt) \quad (10)$$

As the carbon content is 0.04% carbon, the constant ( $K$ ) is calculated to be 21.2. The predictive model for hardness during the tempering process was derived through linear fitting based on the  $P$  tempering parameter. The resulting equation is the following:

$$H = 492.26 - 10.76T(21.1 + \lg t) \quad (11)$$

where ( $H$ ) represents hardness, ( $T$ ) is the tempering temperature, and ( $t$ ) is the tempering time. This model boasts a correlation coefficient of 0.85, demonstrating its high accuracy and reliability in predicting the hardness of low-carbon bainitic steel under various tempering conditions.

In conclusion, the establishment of tempering models based on  $\lambda$  and  $P$  tempering parameters provides a robust framework for predicting the mechanical behavior of low-carbon bainitic steels during the tempering process. These models not only enhance our understanding of the tempering dynamics but also offer practical tools for optimizing heat treatment protocols. Figure 3 illustrates the relationship between hardness and the tempering parameters for low-carbon bainitic steel. The figure clearly demonstrates that hardness after tempering shows a strong linear correlation with the  $\lambda$  and  $P$  tempering parameters, with some deviation observed at lower temperature ranges. This suggests that both parameters are reliable predictors of hardness, but the accuracy may be slightly reduced under low-temperature conditions.

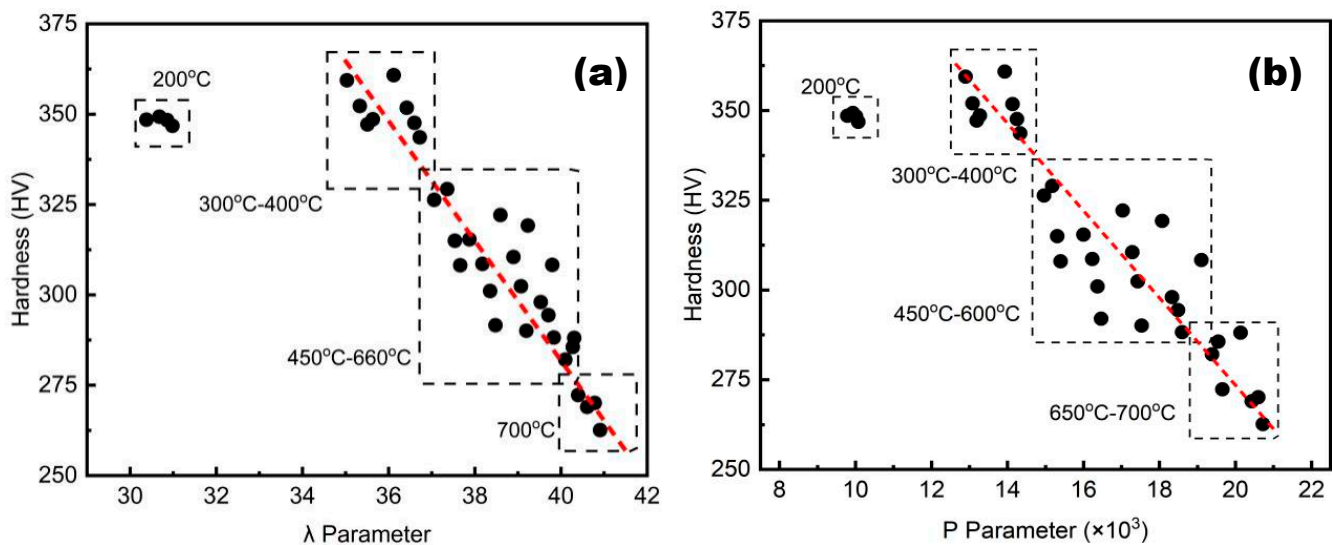


**Figure 3.** Relationship between tempering parameters and hardness: (a) based on  $\lambda$  tempering parameter; (b) based on  $P$  tempering parameter.

In Figure 3a, the hardness is plotted against the  $\lambda$  tempering parameter, revealing a consistent linear relationship across most temperature ranges, except at the lower end where minor deviations occur. Similarly, Figure 3b shows the hardness in relation to the  $P$  tempering parameter, again displaying a predominantly linear trend. These findings underscore the robustness of the tempering models based on the  $\lambda$  and  $P$  tempering parameters in predicting the mechanical properties of the steel. The linear relationships depicted in the graphs affirm the models' effectiveness and highlight the importance of precise temperature control during the tempering process to achieve desired hardness levels. Statistical analysis was conducted to validate the accuracy of the predictive models using metrics such as the  $R$ -squared value and root mean square error (RMSE). The results demonstrated a high level of accuracy, with the  $R$ -squared values for the models based on



the  $P$  and  $\lambda$  tempering parameters being 0.85 and 0.80, respectively. These values indicate a good correlation between the predicted and experimental hardness values. The RMSE values further corroborate the reliability of the models, showcasing their robustness in predicting the tempering behavior of low-carbon bainitic steel.

### 3.3. Error Analysis and Mechanical Prediction

A comprehensive comparison of the measured and calculated hardness values for various tempering processes is depicted in Figures 4 and 5. These figures highlight the accuracy of the prediction models based on the  $\lambda$  and  $P$  tempering parameters.

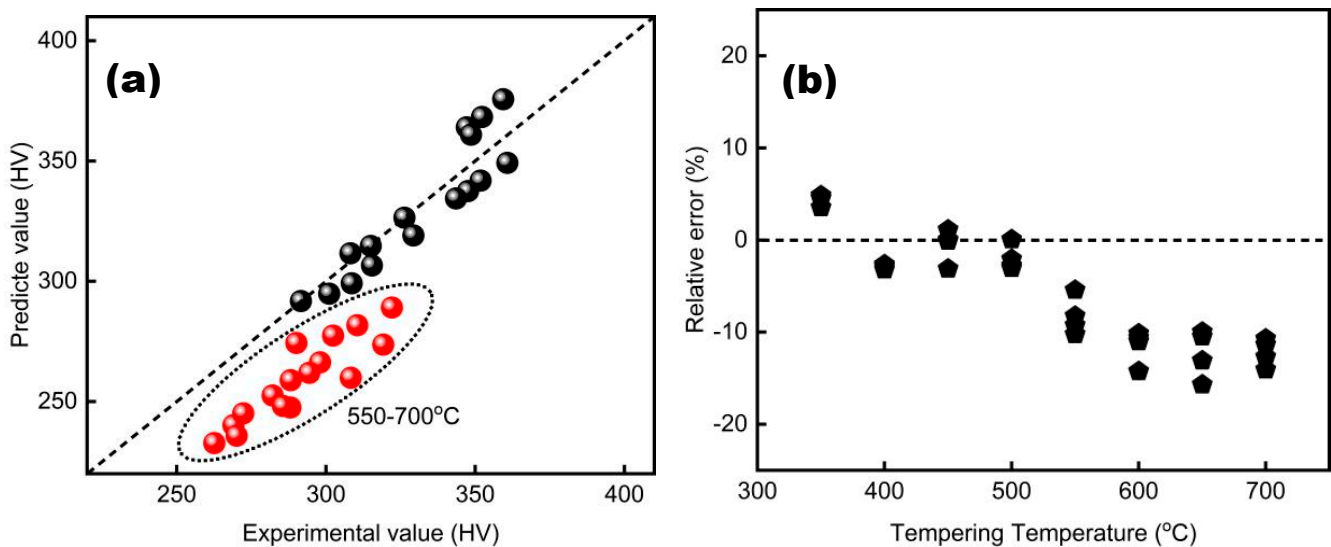


**Figure 4.** Model accuracy analysis based on  $\lambda$  tempering parameter: (a) comparison of calculated and test values; (b) relative error distribution.

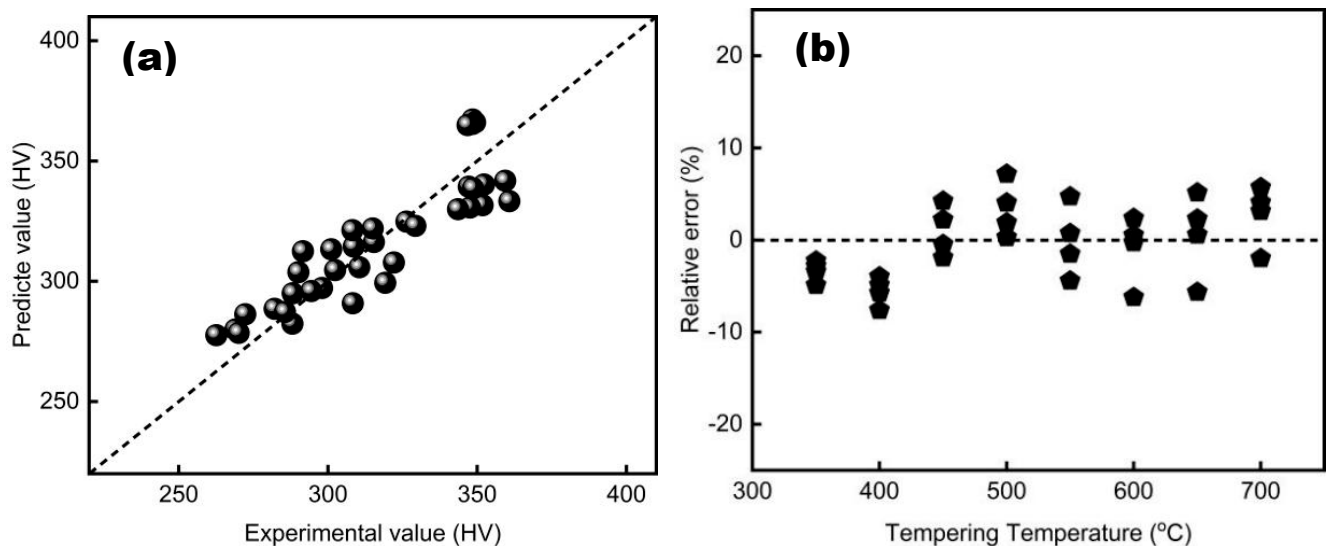


**Figure 5.** Model accuracy analysis based on  $P$  tempering parameter: (a) comparison of calculated and test values; (b) relative error distribution.

In Figure 4a, the comparison between the calculated and experimental hardness values based on the  $\lambda$  tempering parameter demonstrates a strong correlation, indicating the model's reliability. Figure 4b presents the relative error distribution, showing that most errors fall within an acceptable range, confirming the model's precision. The error is less



than 15% for the  $\lambda$  tempering parameter model, showcasing its robustness in predicting hardness accurately across different tempering conditions.

Similarly, Figure 5a illustrates the comparison between calculated and measured hardness values using the  $P$  tempering parameter. The data points align closely along the line of equality, signifying a high degree of accuracy in the model's predictions. Figure 5b shows the relative error distribution for the  $P$ -parameter model, with most errors remaining below 10%. This indicates that the  $P$  tempering parameter model provides a highly accurate prediction of hardness, making it a reliable tool for optimizing tempering processes.

Overall, the error analysis validates that both the  $\lambda$  and  $P$  tempering parameter models can be effectively utilized to predict the mechanical properties of low-carbon bainitic steel during tempering. These models facilitate the optimization of tempering parameters, ensuring desired mechanical properties are achieved consistently. The high correlation coefficients and low error margins underscore the models' applicability in practical settings, enhancing the efficiency and precision of heat-treatment processes.

An equivalent tempering kinetic curves has been developed based on  $\lambda$  tempering parameter models, as shown in Figure 6. This curve allows for a straightforward determination of hardness corresponding to various tempering temperatures and times. For instance, Figure 6 enables direct reading of hardness values for given tempering conditions, facilitating practical applications in industrial settings.

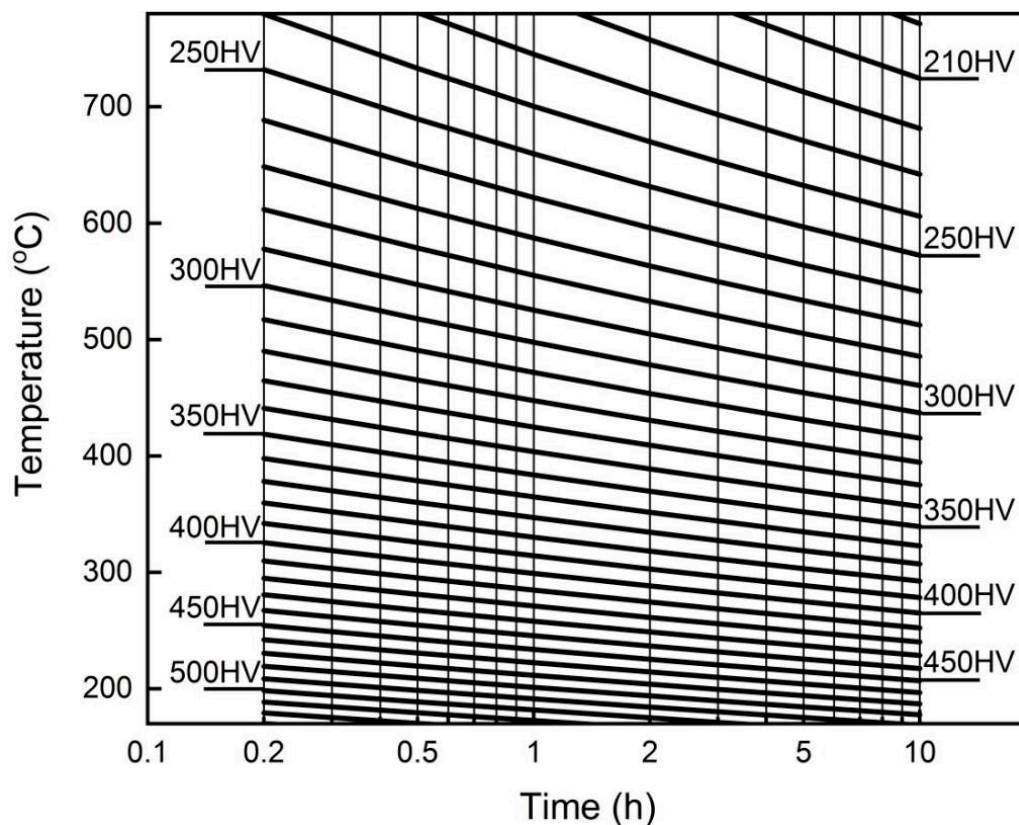


Figure 6. Tempering kinetic curve of equivalent hardness.

The nomogram is plotted based on the  $P$  tempering parameter, which is shown in Figure 7. The nomogram offers a convenient method for adjusting heat treatment processes to achieve desired mechanical properties.

To optimize the tempering process during heat treatment, a nomogram is an effective tool. For example, if the tempering process is initially set at 360 °C for 10 h, this condition is represented by the solid line in Figure 7, intersecting the  $P$  tempering parameter at point M. To further optimize the process, a dashed line is drawn through point M. The intersection of this dashed line with the axes for time ( $t$ ) and temperature ( $T$ ) reveals the

optimized tempering parameters. In this specific case, the optimized parameters would be tempering at 390 °C for 1 h. This adjustment ensures that the same mechanical properties are achieved, owing to the consistent  $p$  value across different tempering conditions. By using this model, it is possible to streamline and enhance the tempering process, ensuring efficiency and precision. The ability to predict and control mechanical properties through such graphical tools is invaluable in industrial applications, where maintaining consistent material performance is crucial.

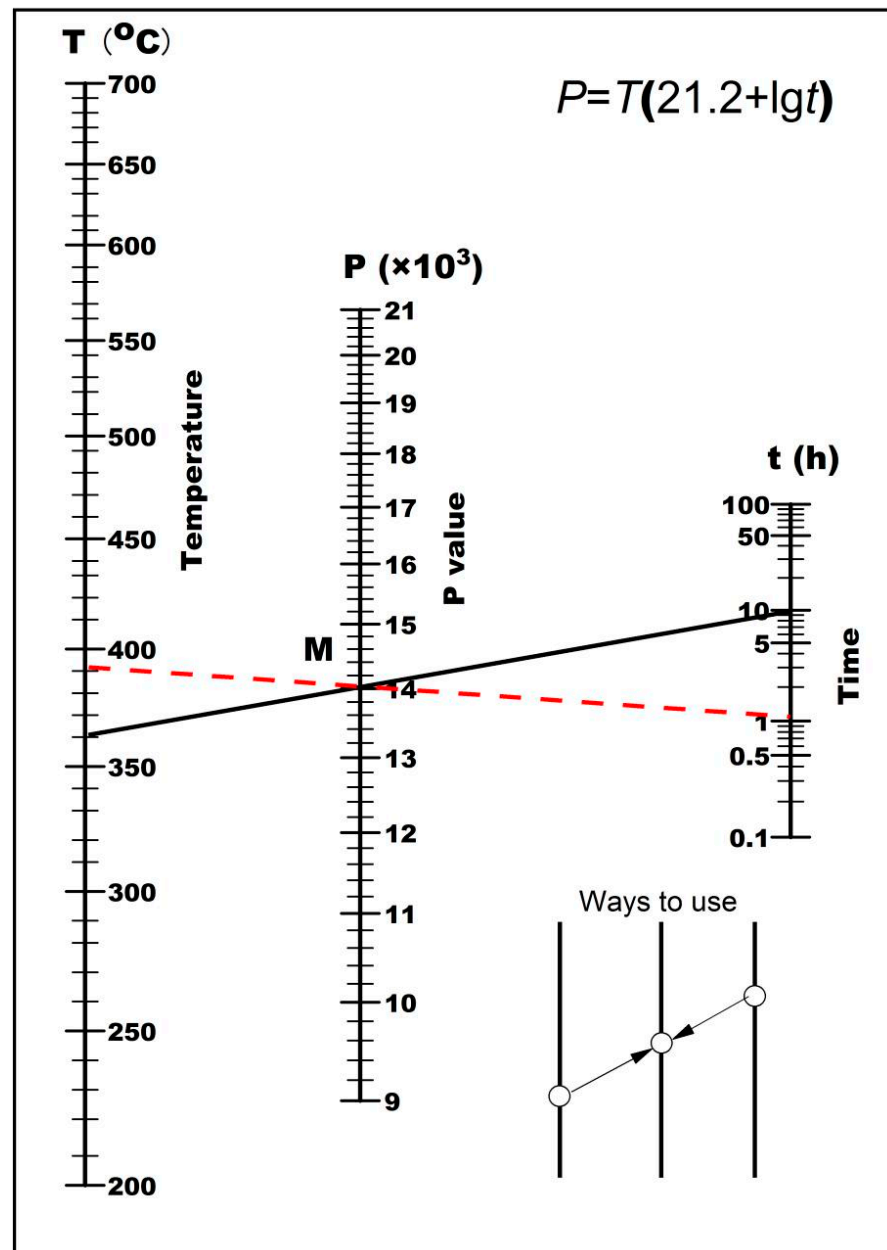


Figure 7. Nomogram of tempering parameters.

Moreover, the use of this nomogram allows for quick adjustments and fine-tuning of the tempering process without extensive trial and error. This not only saves time and resources but also ensures the production of materials with reliable and predictable properties. As a result, engineers can more effectively manage the tempering process to meet specific requirements, enhancing the overall quality and performance of low-carbon bainitic steels in various high-stress applications.

### 3.4. Model Applicability Analysis

To verify and analyze the applicability of the predictive models, the authors investigated the mechanical properties of low-carbon bainitic steels with compositions similar to those studied in this research. For ease of comparison, the strength values reported in the literature were converted to microhardness using empirical formulas, as shown in Table 2. The tempering temperatures and times from these studies were then input into the models developed in this research to obtain predicted hardness values. The comparison of the predicted hardness values with the experimental measurements based on the tempering  $\lambda$  tempering parameter model and the P tempering parameter model are shown in Figure 8.

**Table 2.** Data for Analysis of Tempering Model Applicability.

Tempering Temperature (°C)	Tempering Time (h)	P Model Predicted Hardness	$\lambda$ Model Predicted Hardness	Experimental Hardness	Source
400	1	331.64	312	312.8	[36]
500	1	314.424	298	306.4	[36]
600	1	297.20	291	291.5	[36]
450	0.5	324.81	350.0	341.5	[37]
450	0.5	324.81	341.0	330.6	[37]
450	0.5	324.81	330.0	346.2	[37]
400	1	331.64	320	320.3	[38]
400	5	327.78	340.0	340.2	[38]
400	10	326.12	332	332.2	[38]
400	15	325.15	331.0	331.4	[38]
680	0.5	285.78	252.0	262.4	[39]
680	1	283.42	247.0	257.5	[39]
680	8	276.37	239.0	250.6	[39]

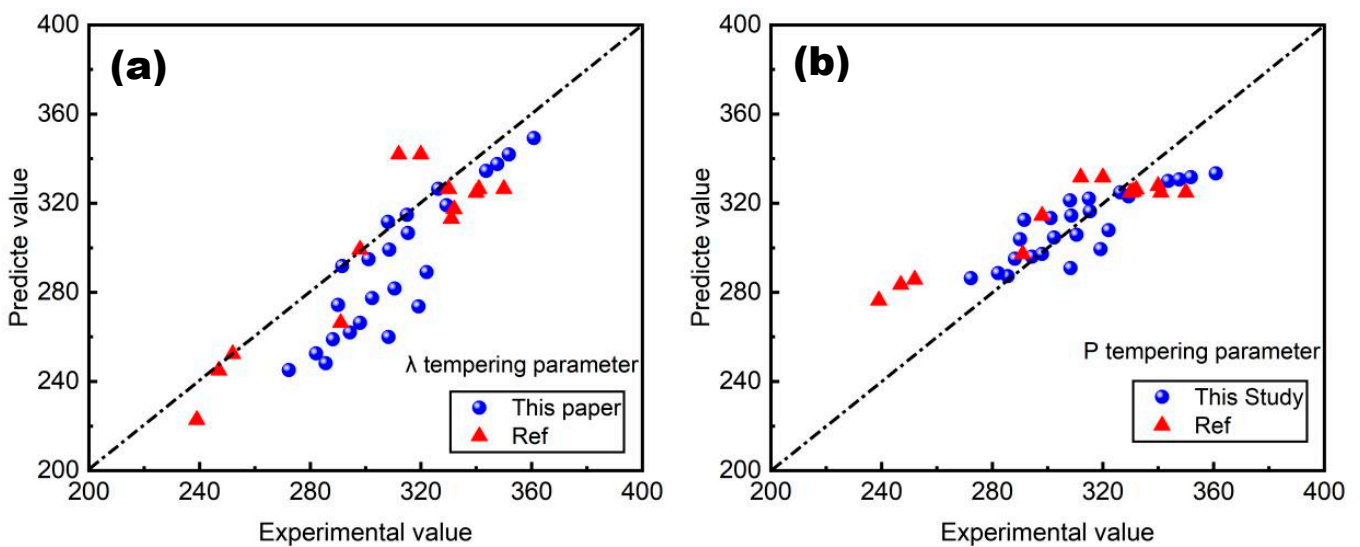


**Figure 8.** Cont.

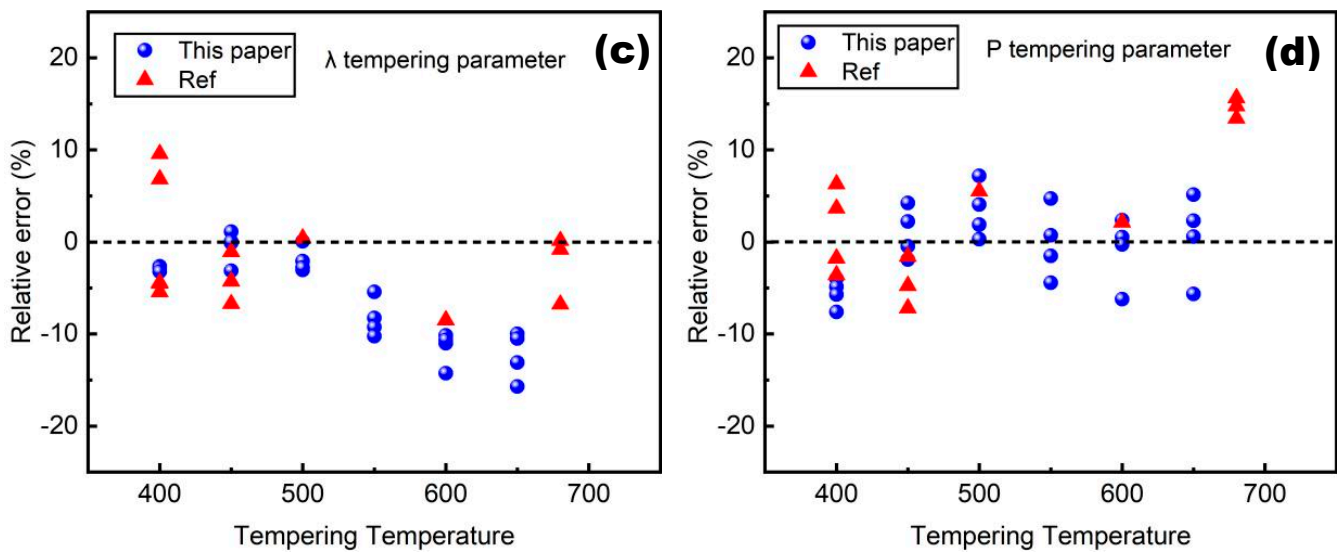


**Figure 8.** Application analysis of tempering models. (a,b) Comparison of calculated and test values; (c,d) relative error distribution.

From the comparison shown in Figure 8a,b, it is evident that the predicted hardness values from both the P model and the  $\lambda$  model exhibit a good correlation with the experimentally measured values. The relative error analysis indicates that when the tempering temperature exceeds 600 °C, the model's prediction accuracy diminishes slightly, with an error margin of about 15%. However, at tempering temperatures below 600 °C, the relative error remains within 10%, demonstrating the robustness and reliability of the predictive models. The analysis confirms that the tempering performance prediction models developed in this study are accurate and can be applied to other materials with similar compositions. This comprehensive approach ensures that the predictive models are not only validated against experimental data but also benchmarked against the established literature, providing a solid foundation for further application and study.

#### 4. Conclusions

In this study, we thoroughly investigated the tempering process of low-carbon bainitic steel to develop robust predictive models for mechanical properties. The key findings are summarized as follows:

1. The tempering activation energy for low-carbon bainitic steel was calculated to be 41.63 cal/mol, using a regression analysis method, specifically employing the least squares technique. This value is critical for understanding the thermal stability and transformation kinetics of the steel during the tempering process.
2. We successfully developed tempering prediction models based on the P and  $\lambda$  tempering parameters. These models integrate the effects of tempering temperature and time, providing a comprehensive framework for predicting the mechanical properties of the steel.
3. Equivalent tempering kinetic curves and nomographs were plotted, allowing for the direct determination of hardness values corresponding to different tempering conditions. These graphical tools facilitate the optimization of tempering parameters, ensuring desired mechanical properties with high accuracy.
4. The predictive models developed in this study offer a reliable method for estimating the hardness of low-carbon bainitic steels. Validation through rigorous statistical analysis has confirmed both their accuracy and applicability. Specifically, the predictive errors for the P tempering parameter model are within 10%, while those for the  $\lambda$  tempering parameter model are within 15%.



**Author Contributions:** Conceptualization, G.S.; methodology, G.S.; formal analysis, Q.W.; investigation, G.S. and Q.W.; writing—original draft preparation, G.S.; writing—review and editing, G.S.; supervision, G.S. All authors have read and agreed to the published version of the manuscript.

**Funding:** This research was funded by financial support from Kunlun Talent Project of Qinghai Province (2023-QLGKLYCZX-032).

**Data Availability Statement:** The data presented in this study are available on request from the corresponding author due to privacy.

**Conflicts of Interest:** The authors declare no conflict of interest.

## References

1. Emi, T. Steelmaking Technology for the Last 100 Years: Toward Highly Efficient Mass-Production Systems for High-Quality Steels. *Tetsu Hagane J. Iron Steel Inst. Jpn.* **2014**, *100*, 31–58. [[CrossRef](#)]
2. Tzevelekou, T.V.; Geck, H.G.; van Hüllen, P.; Höfer, F.; Papamantellos, D.C. Direct smelting of metallurgical dusts and ore fines in a 125t DC-HEP furnace. *Steel Res. Int.* **2004**, *75*, 382–391. [[CrossRef](#)]
3. Liu, H.Y.; Lim, J.; Ma, C. Smelting Period Shortening Practices in Process of Electric Arc Furnace Steelmaking. *Adv. Mater. Res.* **2012**, *572*, 243–248. [[CrossRef](#)]
4. Kuhl, T.; Sun, S.; Trinh, M.K. Equipment and Practice Enhancements at Dofasco’s Vacuum Degas Tank for ULC Steel. *Iron Steel Technol.* **2004**, *1*, 21–27.
5. Shi, X.X.; Zhang, Z.X.; Li, Y.; Zhang, L.L. Bainitic high-phosphorus steel with an excellent combination of strength, toughness and corrosion resistance. *Mater. Lett.* **2023**, *339*, 134088. [[CrossRef](#)]
6. De-Castro, D.; Granados, J.E.; Ramirez, A. Morphological and crystallographic features of granular and lath-like bainite in a low carbon microalloyed steel. *Mater. Charact.* **2022**, *184*, 111703. [[CrossRef](#)]
7. He, S.H.; He, B.B.; Zhu, K.Y.; Huang, M.X. On the correlation among dislocation density, lath thickness and yield stress of bainite. *Acta Mater.* **2017**, *135*, 382–389. [[CrossRef](#)]
8. Caballero, F.G.; Roelofs, H.; Hasler, S.; Capdevila, C.; Chao, J.; Cornide, J.; Garcia-Mateo, C. Influence of bainite morphology on impact toughness of continuously cooled cementite free bainitic steels. *Mater. Sci. Technol.* **2012**, *28*, 95–102. [[CrossRef](#)]
9. Zhang, X.; Liu, S.; Wang, K.; Yan, L.; Wang, J.; Xia, Q.; Yu, H. Effect of vanadium microalloying on phase transformation and strengthening mechanism of 1000 MPa low carbon bainitic steel. *Mater. Sci. Eng. A* **2023**, *884*, 145578. [[CrossRef](#)]
10. Pancholi, V.; Krishnan, M.; Samajdar, I.; Yadav, V.; Ballal, N. Self-accommodation in the bainitic microstructure of ultra-high-strength steel. *Acta Mater.* **2008**, *56*, 2037–2050. [[CrossRef](#)]
11. Im, Y.R.; Oh, Y.J.; Lee, B.J.; Hong, J.H.; Lee, H.C. Effects of carbide precipitation on the strength and Charpy impact properties of low carbon Mn-Ni-Mo bainitic steels. *J. Nucl. Mater.* **2001**, *297*, 138–148. [[CrossRef](#)]
12. Tkachev, E.; Borisov, S.; Borisova, Y.; Kniazuk, T.; Belyakov, A.; Kaibyshev, R. Austenite stabilization and precipitation of carbides during quenching and partitioning (Q&P) of low-alloyed Si-Mn steels with different carbon content. *Mater. Sci. Eng. A* **2024**, *895*, 146212.
13. Shin, S.Y.; Han, S.Y.; Hwang, B.; Lee, C.G.; Lee, S. Effects of Cu and B addition on microstructure and mechanical properties of high-strength bainitic steels. *Mater. Sci. Eng. A* **2009**, *517*, 212–218. [[CrossRef](#)]
14. Canale, L.C.; Yao, X.; Gu, J.; Totten, G.E. A historical overview of steel tempering parameters. *Int. J. Microstruct. Mater. Prop.* **2008**, *3*, 474–525. [[CrossRef](#)]
15. Pashangeh, S.; Somani, M.; Banadkouki, S.S.G. Structure-Property Correlations of a Medium C Steel Following Quenching and Isothermal Holding above and below the  $M_s$  Temperature. *ISIJ Int.* **2021**, *61*, 442–451. [[CrossRef](#)]
16. Rancel, L.; Gómez, M.; Medina, S.F.; Gutierrez, I. Measurement of bainite packet size and its influence on cleavage fracture in a medium carbon bainitic steel. *Mater. Sci. Eng. A* **2011**, *530*, 21–27. [[CrossRef](#)]
17. Adamczyk, J.; Grajcar, A. Heat treatment of TRIP-aided bainitic steel. *Int. J. Microstruct. Mater. Prop.* **2007**, *2*, 112–123. [[CrossRef](#)]
18. Dong, Y.; Lan, X.; Yang, S.; Lu, J.; Yan, S.; Wei, K.; Wang, Z. Effect of quenching and tempering treatments on microstructure and mechanical properties of 300 M ultra-high strength steel fabricated by laser powder bed fusion. *Mater. Charact.* **2024**, *212*, 113935. [[CrossRef](#)]
19. Ma, S.; Zhang, C.; Zhang, J.; Liu, H.; Huang, Y. Achieving high strength-ductility synergy in nickel aluminum bronze alloy via a quenching-aging-tempering heat treatment. *Mater. Lett.* **2023**, *333*, 133661. [[CrossRef](#)]
20. Zhang, J.; Dai, Z.; Zeng, L.; Zuo, X.; Wan, J.; Rong, Y.; Chen, N.; Lu, J.; Chen, H. Revealing carbide precipitation effects and their mechanisms during quenching-partitioning-tempering of a high carbon steel: Experiments and Modeling. *Acta Mater.* **2021**, *217*, 117176. [[CrossRef](#)]
21. Koyanbayev, Y. Applying the Hollomon-Jaffe parameter to predict changes in mechanical properties of irradiated austenitic chromium-nickel steels during isothermal exposure. *AIMS Mater. Sci.* **2024**, *11*, 216–230. [[CrossRef](#)]
22. Virtanen, E.; Van Tyne, C.J.; Levy, B.S.; Brada, G. The tempering parameter for evaluating softening of hot and warm forging die steels. *J. Mater. Process. Technol.* **2013**, *213*, 1364–1369. [[CrossRef](#)]

23. Kang, S.; Lee, S.J. Prediction of Tempered Martensite Hardness Incorporating the Composition-Dependent Tempering Parameter in Low Alloy Steels. *Mater. Trans.* **2014**, *55*, 1069–1072. [[CrossRef](#)]
24. Revilla, C.; López, B.; Rodríguez-Ibabe, J.M. Carbide size refinement by controlling the heating rate during induction tempering in a low alloy steel. *Mater. Des.* **2014**, *62*, 296–304. [[CrossRef](#)]
25. Hoja, S.; Hoffmann, F.; Steinbacher, M.; Zoch, H.W. Investigation of the Tempering Effect during Nitriding. *HTM Z. Fur Werkst. Warmebehandl. Fert.* **2018**, *73*, 335–343. [[CrossRef](#)]
26. Salas Vicente, F.; Carcel Carrasco, J.; Fernández Antoni, R.; Ferrero Taberner, J.C.; Pascual Guillamón, M. Hardness Prediction in Quenched and Tempered Nodular Cast Iron Using the Hollomon-Jaffe Parameter. *Metals* **2021**, *11*, 297. [[CrossRef](#)]
27. Fujita, K.; Ueda, M.; Ikeda, M.; Hayashi, K. Monitoring of Tempering Behavior in Fe-C-Mn Alloys by Precise Measurement of Electrical Resistivity. *Adv. Mater. Res.* **2014**, *922*, 173–176. [[CrossRef](#)]
28. Gomes, C.; Kaiser, A.L.; Bas, J.P.; Aissaoui, A.; Piette, M. Predicting the mechanical properties of a quenched and tempered steel thanks to a “tempering parameter”. *Metall. Res. Technol.* **2010**, *107*, 293–302. [[CrossRef](#)]
29. Nagasaka, T.; Ando, M.; Tanigawa, H.; Sakasegawa, H.; Tanaka, T.; Muroga, T.; Sagara, A. Tensile properties of F82H steel after aging at 400–650 °C for 1000–30,000 h. *Fusion Eng. Des.* **2017**, *124*, 1011–1014. [[CrossRef](#)]
30. Inoue, T. A New Tempering Parameter and Its Application to the Integration of Tempering Effect of Continuous Heat Cycle. *Tetsu Hagane* **2009**, *66*, 1532–1541. [[CrossRef](#)]
31. Tamaki, K.; Suzuki, J. Time-Temperature-Hardness Diagrams of Tempered Steels. *Res. Rep. Fac. Eng. Mie Univ.* **1990**, *15*, 9–22.
32. Dong, H.; Zhang, Y.; Miyamoto, G.; Inomoto, M.; Chen, H.; Yang, Z.; Furuhashi, T. Unraveling the effects of Nb interface segregation on ferrite transformation kinetics in low carbon steels. *Acta Mater.* **2021**, *215*, 117081. [[CrossRef](#)]
33. Takahashi, J.; Kawakami, K.; Hamada, J.-I.; Kimura, K. Direct observation of niobium segregation to dislocations in steel. *Acta Mater.* **2016**, *107*, 415–422. [[CrossRef](#)]
34. Goulas, C.; Kumar, A.; Mecozzi, M.G.; Castro-Cerda, F.M.; Herbig, M.; Petrov, R.H.; Sietsma, J. Atomic-scale investigations of isothermally formed bainite microstructures in 51CrV4 spring steel. *Mater. Charact.* **2019**, *152*, 67–75. [[CrossRef](#)]
35. Jun, H.J.; Park, S.H.; Choi, S.D.; Park, C.G. Decomposition of retained austenite during coiling process of hot rolled TRIP-aided steels. *Mater. Sci. Eng. A* **2004**, *379*, 204–209. [[CrossRef](#)]
36. Guo, A.; Song, X.; Tang, J.; Yuan, Z. Effect of tempering temperature on the mechanical properties and microstructure of an copper-bearing low carbon bainitic steel. *J. Univ. Sci. Technol. Beijing* **2008**, *1*, 40–44. [[CrossRef](#)]
37. Wang, G.T.; Zhou, Y.L.; Wang, L.J.; Liu, C.M. Study on Microstructures and Properties of Low-Carbon-Steel Heavy Plate Treated by Quenching and Dynamic Partitioning. *J. Mater. Eng. Perform.* **2022**, *31*, 1195–1203. [[CrossRef](#)]
38. Liang, Z.; Wang, J.; Li, H.; Zhang, X.; Liu, C.; Sun, D.; Yang, Z.; Zhang, F. Microstructure evolution of V-containing low carbon ultra-fine bainitic steel during medium-temperature tempering and strengthening-toughening mechanism. *Mater. Sci. Eng. A* **2024**, *901*, 146566. [[CrossRef](#)]
39. Chen, Y.W.; Huang, B.M.; Tsai, Y.T.; Tsai, S.P.; Chen, C.Y.; Yang, J.R. Microstructural evolutions of low carbon Nb/Mo-containing bainitic steels during high-temperature tempering. *Mater. Charact.* **2017**, *131*, 298–305. [[CrossRef](#)]

**Disclaimer/Publisher’s Note:** The statements, opinions and data contained in all publications are solely those of the individual author(s) and contributor(s) and not of MDPI and/or the editor(s). MDPI and/or the editor(s) disclaim responsibility for any injury to people or property resulting from any ideas, methods, instructions or products referred to in the content.